J. Fluid Mech. (1990), *vol.* 218, *pp.* 641–658
Printed in Great Britain

Instability of a viscous liquid jet surrounded by a viscous gas in a vertical pipe

By S. P. LIN AND E. A. IBRAHIM
Department of Mechanical and Aeronautical Engineering, Clarkson University, Potsdam, NY 13676, USA

(Received 27 June 1989 and in revised form 6 March 1990)

The instability of a cylindrical liquid jet encapsulated by a viscous gas in a pipe is analysed in a parameter space spanned by the Reynolds number, the Froude number, the Weber number, the density ratio, the viscosity ratio, and the diameter ratio. A convergent solution of the problem is constructed by a Galerkin projection with two orthogonal sets of functions. Two distinctively different modes of instability are obtained. The first is the Rayleigh mode which tends to break up the jet into drops of diameter comparable with the jet diameter. The amplification rate of the disturbance belonging to this mode depends weakly on all parameters except the Weber number which represents the ratio of the surface tension force to the inertia force at the interface. The mechanism of the instability remains that of capillary pinching even in the presence of a viscous gas and gravity. However, the surface tension is stabilizing in the other mode termed the Taylor mode. The Taylor mode instability is due to the pressure and shear fluctuations at the interface. This mode tends to produce droplets of diameters much smaller than that of the jet. It is shown that the former mode appears when the Weber number is much larger than the gas to liquid density ratio. When this ratio is of order one, the instability can be due to either modes depending on the values of the rest of the parameters. When the density ratio is much larger than the Weber number, Taylor's atomization mode replaces the Rayleigh mode.

1. Introduction

The instability of an inviscid liquid jet with respect to temporally growing disturbances in the absence of gravity and ambient gas was analysed by Rayleigh (1879). He showed that the disturbance possessing the maximum amplification rate could cause the jet to break up to form droplets comparable in size with the jet diameter. Chandrasekhar (1961) showed that the neglected liquid viscosity can only reduce the amplification rate of disturbances but cannot suppress the instability caused by capillary pinching. The convective and absolute instability of a liquid jet was investigated by Keller *et al.* (1972), Leib & Goldstein (1986*a*, *b*), and Lin & Lian (1989). Taylor (1963), Lin & Kang (1987), and Lin & Lian (1990), showed that when the gas to liquid density ratio, Q, is much greater than the Weber number, a viscous jet of radius R_1 may actually become unstable with respect to disturbances of wavelength $\lambda \ll R_1$. Lin & Creighton (1990) found that while the mechanism of Rayleigh's instability is capillary pinching, the mechanism of Taylor's mode is the interfacial pressure fluctuation. However, the effects of the interfacial shear on the Rayleigh and the Taylor modes of the jet instability remain unknown, since the gas viscosity is neglected in all of the above mentioned theories. The effect of the

viscosity of a motionless surrounding fluid on the break-up of a motionless viscous cylindrical thread was investigated theoretically by Tomotika (1934). The break-up mechanism for this case remains capillary pinching.

Joseph, Renardy & Renardy (1984) investigated the instability of two immiscible liquids of the same density but of different viscosities in a pipe. The interfacial tension was neglected. The effects of surface tension and density stratification in the absence of gravity were later included in the investigations of Preziosi, Chen & Joseph (1989) and Hu & Joseph (1989). Smith (1989) investigated the instability of two immiscible fluids of the same viscosity but of different densities in a vertical pipe. These works are of fundamental importance, because they isolate the effects of the density and viscosity discontinuities at the interface. However, they cannot be applied to elucidate the coupled effects of surface tension, interfacial shear, gravitational acceleration and pressure fluctuation on the Rayleigh and the Taylor modes of instability.

A stability theory of a viscous liquid jet surrounded by a viscous gas in a vertical pipe in the presence of gravity and interfacial tension is formulated in §2. A convergent method of solution by orthogonal expansion is developed in §3. In §4, results showing the effects of relevant parameters are presented and discussed in relation to some known experiments and theories. A perspective of the present work is given in the conclusion section. While this paper was being reviewed, Professor O. M. Phillips informed us that another paper on the same subject had been submitted to the *Journal of Fluid Mechanics* by Chen, Bai & Joseph (1990). However, the results were reported for a different range of parameters. While our results are relevant to the atomization of a liquid jet forced into the ambient gas, their results for forced flows do not include the parameter range in which the most amplified waves scale with the capillary length which is the ratio of the surface tension to the inertia force per unit volume of gas at the interface.

2. Formulation of the problem

Consider the stability of a cylindrical liquid jet of radius R_1. The jet is surrounded by a viscous gas enclosed in a vertical circular pipe of radius R_2 which is concentric with the jet. For the jet to maintain a constant radius the pressure gradient in the steady liquid- and the gas-flows must remain the same constant. This will allow the pressure force difference across the liquid–gas interface to be exactly balanced by the surface tension force as required. Such coaxial flows of liquid and gas, in the presence of gravity, which satisfy exactly the Navier–Stokes equations are given by

$$\left.\begin{aligned} W_1(r) &= -1+\frac{Nr^2}{[N-(1-l^2)]}\left\{1-\frac{(1-Q)}{4N}\frac{Re}{Fr}[2\ln l+(1-l^2)]\right\}, \\ W_2(r) &= -\frac{(l^2-r^2)}{[N-(1-l^2)]}\left\{1-\frac{(1-Q)}{4N}\frac{Re}{Fr}[2\ln l+(1-l^2)]\right\} \\ &\quad +\frac{(1-Q)}{4N}\frac{Re}{Fr}\left[l^2-r^2-2\ln\left(\frac{l}{r}\right)\right], \end{aligned}\right\} \tag{1}$$

where

$$N=\frac{\mu_2}{\mu_1},\quad l=\frac{R_2}{R_1},\quad Q=\frac{\rho_2}{\rho_1},$$

$$Re \equiv \text{Reynolds number} = \rho_1 W_0 R_1/\mu_1,$$

$$Fr \equiv \text{Froude number} = W_0^2/gR_1,\quad R = Re/Fr,$$

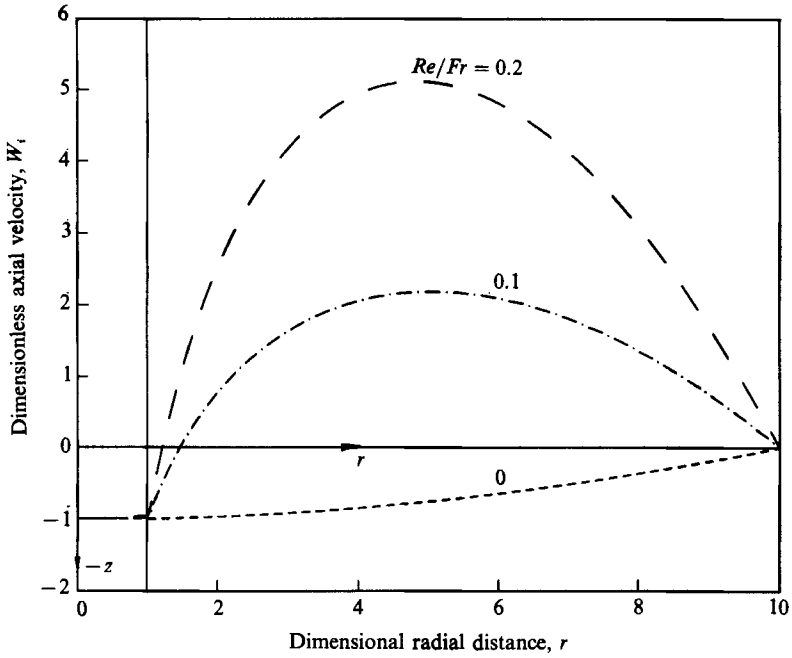

FIGURE 1. Velocity distribution. $Q = 0.0013$, $N = 0.018$, $l = 10$.

where the subscript 1 or 2 stands for the liquid or the gas phase respectively, W_0 is the magnitude of the jet velocity in the z-axis (cf. figure 1), r is the radial distance normalized with R_1, $W(r)$ is the axial velocity distribution, μ is the dynamic viscosity, ρ is density, and g is the gravitational acceleration in the negative z-direction. Some velocity distributions in a water jet and in the surrounding air flow under one atmosphere are given in figure 1 for various values of Re/Fr. Note the large difference in the slopes of the velocity profiles in the liquid and the gas phases due to the large difference in their viscosity, when R is relatively large.

The stability of the basic state described by (1) with respect to a normal mode axisymmetric disturbance is governed by the well-known Orr–Sommerfeld equation (Drazin & Reid 1981),

$$[\omega - (N'/Re)\,\mathrm{D}^2]\,\mathrm{D}^2\phi_i(r) + \mathrm{i}kW_i(r)\,\mathrm{D}^2\phi_i(r) - \mathrm{i}kr\,\mathrm{d}[\mathrm{d}W_i(r)/r]\,\phi_i = 0 \quad (i = 1, 2), \quad (2)$$

$$\mathrm{D}^2 = \mathrm{d}^2 - r^{-1}\mathrm{d} - k^2, \quad \mathrm{d} = \mathrm{d}/\mathrm{d}r, \quad N' = \nu_i/\nu_1,$$

where ν is the kinematic viscosity, the subscript i stands for the liquid phase or the gas phase depending on if $i = 1$ or $i = 2$, ω and k are respectively the dimensionless complex frequency and the wavenumber of the disturbance, and ϕ_i is the amplitude of the normal mode disturbance related to the Stokes stream function ψ_i by

$$\psi_i(r, z, t) = \phi_i(r)\,\mathrm{e}^{(\mathrm{i}kz + \omega t)},$$

where t is time normalized with R_1/W_0. The Stokes stream function is related respectively to the radial and axial components of the disturbance velocity by

$$u_i = \psi_{iz}/r, \quad w_i = -\psi_{ir}/r,$$

where the subscripts z and r denote partial differentiations.

The boundary conditions at the perturbed liquid–gas interface $r = 1 + \eta$ can be linearized by use of the Taylor series expansions of all variables involved about

$r = 1$, and retaining only terms of the first order in perturbations. Hence, the interfacial conditions are to be evaluated at $r = 1$ with η as an additional unknown. Since the interface is a material surface, η must satisfy at $r = 1$ the kinematic condition

$$\eta_t + W_i \eta_z = \psi_{iz}.$$

Other interfacial kinematic conditions are the continuity of the radial and tangential components of the velocity across the interface given respectively by

$$[\psi_{iz}]_2^1 \equiv [\psi_{1z} - \psi_{2z}]_{r=1} = 0,$$

$$[W_{ir}\eta - \psi_{ir}]_2^1 = 0.$$

The balancing of forces per unit area of the interface in the tangential and normal directions leads respectively to the dynamic conditions at $r = 1$,

$$[N_i\{\eta W_{irr} - (\psi_{ir}/r)_r + \psi_{izz}\}]_2^1 = 0,$$

$$[p_i - (2/Re)\, N_i(\psi_{iz}/r)_r]_2^1 + (\eta + \eta_{zz})\, We = 0,$$

where p_i is the disturbance pressure,

$$We \equiv \text{Weber number} = S/\rho_1 W_0^2 R_1, \quad N_i = \mu_i/\mu_1,$$

in which S is the surface tension. Thus, We signifies the ratio of surface tension force to the inertia force per unit area of the interface. Chandrasekhar's surface tension parameter, $J \equiv SR_1/\rho_1 \nu_1^2$, was used by Preziosi *et al.* and Lin & Lian (1990). The use of this parameter may have the advantage that a small error in measuring Re will not be magnified in We. However, one is denied this advantage when one is concerned with atomization. The condition for atomization is $We \ll Q$ (cf. Lin & Lian 1990). In terms of J, this condition is $J \ll Re^2 Q$. Thus the error made in measuring Re will again be magnified by a power of 2 when one delineates the atomization regime in $J \sim Re^2 Q$ space. The propagation of an error in experiments cannot be always avoided by simply defining a new parameter. The boundary condition at the pipe wall is the no-slip condition at $r = 1$,

$$\psi_{2z} = 0, \quad \psi_{2r} = 0.$$

The normal mode axisymmetric pressure disturbance and interfacial displacement are written as

$$[p_i, \eta] = [\zeta_i(r), \xi]\, e^{(ikz+\omega t)}. \tag{3}$$

Substituting (3) and the normal mode of ψ_i into the above boundary conditions, we rewrite them in the same order of appearance

$$(\omega + ikW_1)\,\xi - ik\phi_1 = 0, \tag{4a}$$

$$[\phi_i]_2^1 = 0, \tag{4b}$$

$$[\xi W_{ir} - \phi_{ir}]_2^1 = 0, \tag{4c}$$

$$[N_i B\phi_i]_2^1 - (1-Q)\, R\xi = 0, \tag{4d}$$

$$B = \mathrm{d}^2 - \mathrm{d}/r + k^2,$$

$$[\zeta_i - (2ik/Re)\, N_i(\phi_{ir} - \phi_i)]_2^1 + \xi(1-k^2)\, We = 0, \tag{4e}$$

$$\phi_{2r}(l) = 0, \tag{4f}$$

$$\phi_2(l) = 0. \tag{4g}$$

The last term in (4*d*) arises from the second derivatives of the basic flows. The pressure amplitude discontinuity in (4*e*) can be obtained from the linearized Navier–Stokes equations, and are found to be

$$[\zeta_i]_2^1 = [Q_i\{(\omega+\mathrm{i}kW_i)\,\phi_{ir}-\mathrm{i}kW_{ir}\,\phi_i\}-N_i(\mathrm{D}^2\phi_i)_r/Re]_2^1\,(\mathrm{i}k)^{-1} \quad (Q_i=\rho_i/\rho_1).$$

Non-trivial solutions of (1) with its boundary conditions (4*a*)–(4*g*) for given flow parameters Re, Fr, We, Q, N, l and k exist only for certain eigenvalues ω. The real part of ω determines the stability of the flow, and the imaginary part of ω determines the characteristic frequency of the disturbance.

3. Solution by orthogonal expansions

The solution of the problem formulated in the previous section will be expanded in an orthogonal set of functions in each of the flow fields in the liquid and in the gas (lighter incompressible fluid). The two orthogonal sets are associated with the same differential operator in (2), i.e. D^2, but with different domain boundaries. By use of the change of variable

$$\phi_i = rf_i \quad (i=1,2),$$

we have $$\mathrm{D}^2\phi_i = r(L-k^2)f_i,$$

where $$L = r^{-1}\,\mathrm{d}(r\,\mathrm{d})-r^{-2}.$$

The orthogonal functions will be chosen among the solutions of the Bessel equation of the first order with the parameter k_{in}

$$(L^2+k_{in}^2)\,F_{in} = 0 \quad (n=1,2,\ldots,M_i), \tag{5}$$

where F_{in} stands for $F_i(k_{in}r)$, and M_i is an arbitrary large integer. The bounded solutions of (5) which form an orthogonal set of functions in $r \leqslant 1$ are

$$F_{1n} = J_1(k_{1n}r), \tag{6}$$

where k_{1n} are the roots of

$$k_{1n}\,J_0(k_{1n})-J_1(k_{1n}) = 0. \tag{7}$$

With these values of k_{1n}, we have

$$\int_0^1 rF_{1m}F_{1n} = \delta_{mn}^{(1)} \tag{8}$$

where $\delta_{mn}^{(1)} = 0$ if $m \neq n$, if $m = n$ it is given by

$$\delta_{nn}^{(1)} = 0.5(k_{in}^2-1)\,J_0^2(k_{1n}). \tag{9}$$

The bounded solutions of (5) which form an orthogonal set of functions in the domain $1 \leqslant r \leqslant l$ are

$$F_{2n} \equiv F_2(k_{2n}r) = Y_1(k_{2n}l)\,J_1(k_{2n}r)-J_1(k_{2n}l)\,Y_1(k_{2n}r), \tag{10}$$

where k_{2n} are the roots of

$$F_2(k_{2n})-k_{2n}\bar{F}(k_{2n}) = 0, \tag{11}$$

$$\bar{F}(k_{2n}r) = J_0(k_{2n}r)\,Y_1(k_{2n}l)-J_1(k_{2n}l)\,Y_0(k_{2n}r). \tag{12}$$

With the values of k_{2n} thus determined, we have

$$\int_1^l rF_{2n}F_{2m}\,\mathrm{d}r = \delta_{mn}^{(2)}, \tag{13}$$

where $\delta^{(2)}_{mn} = 0$ if $m \equiv n$, otherwise it is given by the integral on the left-hand side of the above equation with F_{2n} given by (10). Note that

$$F_2(k_{2n} l) = 0. \tag{14}$$

We now expand the eigenvector in a truncated series of the above orthogonal functions

$$\phi_i = r a_{in} F_{in} \quad (i = 1, 2), \tag{15}$$

where the repeated indices n denote summation over $n = 1$ to $n = M_i\,(i = 1, 2)$. The number of terms M_i required in the two-flow domains may not be the same for the required accuracy. The components of the eigenvector will be obtained by use of the Galerkin projection. The following formula which can be derived with integration by parts will be used repeatedly in the reduction of the Galerkin projection,

$$\int_{s_i}^{t_i} rGL(g)\,\mathrm{d}r = \int_{s_i}^{t_i} rgL(G)\,\mathrm{d}r - [rg\,\mathrm{d}(G) - rG\,\mathrm{d}(g)]_{s_i}^{t_i}, \tag{16}$$

where g and G are functions of r. The Galerkin projection of (2) gives

$$\int_{s_i}^{t_i} rF_{im}[(L-k^2-Re\,\omega')(L-k^2)f_i + ik(\nu_1/\nu_i)Re\,W_i(L-k^2)f_i]\,\mathrm{d}r = 0, \tag{17}$$

where $\omega' = \omega(\nu_1/\nu_i)$ $s_1 = 0$, $t_1 = s_2 = 1$, and $t_2 = l$. By use of (16), the orthogonality conditions, and the following relations

$$[rL(f_1)\,\mathrm{d}(F_{1m}) - rF_{1m}\,\mathrm{d}L(f_1)]_{r=s_1} = 0,$$

$$F_2(k_{2m} t_2) = 0,$$

we can reduce (17) to

$$\begin{aligned} &e_{imn} a_{in} - \nu t_1 \delta_{1i}[(\mathrm{d}F_{1m})_{t_1}\alpha - (F_{1m})_{t_1}\beta] \\ &- \nu s_2 \delta_{2i}[(t_2/s_2)(\mathrm{d}F_{2m})_{t_2}\gamma + (F_{2m})_{s_2}\delta - (\mathrm{d}F_{2m})_{s_2}\epsilon] = 0 \quad (m, n = 1, 2, \ldots, M_i), \end{aligned} \tag{18}$$

where $\nu = (\nu_i/\nu_1)$, the subscripts in the parentheses denote the values of r at which the parenthesized functions are to be evaluated, and

$$\begin{aligned} e_{imn} = {} & \delta^{(t)}_{mn}[k^2(\nu k^2 + Re\,\omega) + (2\nu k^2 + Re\,\omega)k^2_{im} + \nu(k_{in}\,k_{im})^2] \\ & + \mathrm{i}k\,Re\,(k^2 + k^2_{in}) \int_{s_i}^{t_i} rW_i F_{im} F_{in}\,\mathrm{d}r - \mathrm{i}k\delta_{2i}[(1-Q)R\,Re/N] \int_{s_2}^{t_2} F_{im} F_{in}\, r^{-1}\,\mathrm{d}r, \end{aligned}$$

$$\alpha = [L(f_1)]_{t_1}, \quad \beta = [\mathrm{d}L(f_1)]_{t_1},$$

$$\gamma = [L(f_2)]_{t_2}, \quad \delta = [\mathrm{d}L(f_2)]_{s_2}, \quad \epsilon = [L(f_2)]_{s_2}. \tag{19}$$

It is known that termwise differentiations of truncated series representations of functions do not provide as high an accuracy for the derivatives of functions as for functions themselves. For this reason we treat α to ϵ in (18), which involve derivatives higher than second, as five additional unknowns. Thus (18) is a system of $M_1 + M_2$ equations in $M_1 + M_2 + 5$ unknowns. The required additional equations are provided by the six boundary conditions (4a)–(4f) which contain an additional unknown ξ. Note that boundary condition (4g) is already satisfied, because of (14).

Substituting the series solution (15) into (4*a*) to (4*f*) we have

$$\mathrm{i}kF_1(k_{1n})\,a_{1n}-[\omega+\mathrm{i}kW_1(1)]\,\xi=0, \tag{20a}$$

$$[a_{in}\,F_{in}]_2^1=0, \tag{20b}$$

$$[\xi W_{ir}-a_{in}(F_{in}+\mathrm{d}F_{in})]_2^1=0, \tag{20c}$$

$$[N_i\{(k^2-1)\,F_{in}+\mathrm{d}F_{in}+\mathrm{d}^2F_{in}\}\,a_{in}]_2^1-(1-Q)\,\xi=0, \tag{20d}$$

$$\begin{aligned}[\{(\omega+\mathrm{i}kW_1)\,Re\,Q_i(F_{in}+\mathrm{d}F_{in})-\mathrm{i}k\,Re\,Q_i\,W_{ir}\,F_{in}\\ +N_i[(k^2+k_{in}^2)\,F_{in}+(3k^2+k_{in}^2)\,\mathrm{d}F_{in}]\}\,a_{in}]_2^1+\mathrm{i}k\,Re\,We\,(1-k^2)\,\xi=0,\end{aligned} \tag{20e}$$

$$(\mathrm{d}F_{2n})_l\,a_{2n}=0. \tag{20f}$$

Equation (18) and the above boundary conditions form a system of (M_1+M_2+6) homogeneous linear equations in the same number of unknowns. Making the following identifications

$$a_{1n}=X_n \quad (n=1,\ldots,M_1),$$

$$a_{2n}=X_{n+M_1} \quad (n=1,\ldots,M_2), \quad M=M_1+M_2,$$

$$(\alpha,\beta,\gamma,\delta,\epsilon,\xi)=(X_{M+1},X_{M+2},X_{M+3},X_{M+4},X_{M+5},X_{M+6}),$$

this linear homogeneous system can be written in a standard form

$$(A_{mn}+\omega B_{mn})\,X_n=0 \quad (m,n=1,2,\ldots,M+6),$$

where the elements of matrices A_{mn} and B_{mn} can be identified easily from (18) and the above boundary conditions. A non-trivial solution up to an arbitrary multiplicative constant of this system exists only if the determinant of its coefficient matrix vanishes, i.e.

$$|A_{mn}+\omega B_{mn}|=0. \tag{21}$$

To construct the eigenfunctions of the original system, which is not required in this work, we need only the eigenvectors a_{1n} and a_{2n}. The values of α, β, γ, δ, ϵ and ξ are not required. The explanation of the numerical computation involved in the solution of (21) is in order. All computations are carried out, in double precision with Gould PN 9780 at Clarkson and the supercomputer facility at the Cornell Theory Center. To construct the orthogonal functions F_i, we solve (7) and (11) with (12) respectively for k_{1n} and k_{2n} with the Muller (1956) method. All integrals involved, in (18) except $\delta_{mn}^{(1)}$ which has a closed form expression, are evaluated with the Gauss–Kronrod quadrature. For a given set of parameters (*Re*, *We*, *Fr*, *Q*, *N*, *l*) the eigenvalue ω is obtained from (21) for various values of k with the method by Kaufman (1974). In this complex eigenvalue solution, M_1 and M_2 are systematically increased until the eigenvalue corresponding to the most amplified or the least damped disturbance converges to the desired significant digits.

4. Results

Table 1 gives a typical example which demonstrates the convergence of the method of determining the eigenvalues for a given set of flow parameters. It is seen that as M_1 and M_2 are increased respectively from 6 and 54 to 7 and 63, the eigenvalues remains the same up to the first four significant digits. Note that when $M_1=7$ and $M_2=63$ there are 76 eigenvalues for the given set of parameters. Only the one corresponding to the most amplified disturbance is given in the table. The same

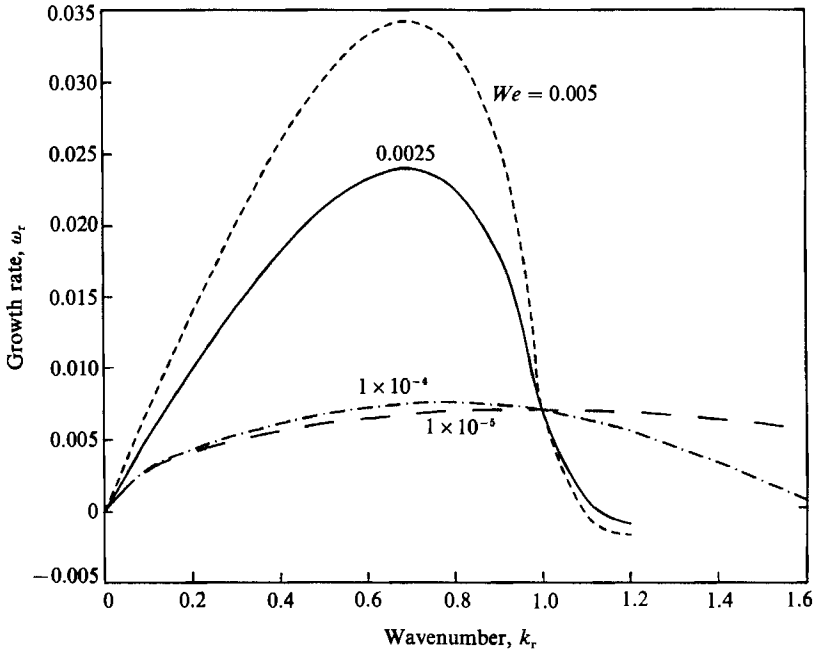

FIGURE 2. Destabilizing effect of surface tension on the Rayleigh mode. $Q = 0.0013$, $N = 0.018$, $l = 10$, $R = 0$, $Re = 400$.

M_1	M_2	ω_r	ω_i
3	15	0.0238	0.7003
5	35	0.0239	0.7013
5	45	0.0239	0.7017
6	54	0.0239	0.7021
7	63	0.0239	0.7021

TABLE 1. Convergence to the most amplified mode. $k = 0.7$, $We = 0.0025$, $Re = 400.0$, $Re/Fr = 0$, $Q = 0.0013$, $l = 10.0$, $N = 0.018$

convergence test was carried out for every computation for the most amplified or the least damped eigenvalues for various sets of parameters reported in this work. Preziosi *et al.* (1989) used Chebyshev polynomials as base functions for their solution of a special case of zero gravity in the present problem. They required 80 terms for satisfactory convergent results. Thus the terms required in the present problem with gravitational effect is slightly less than that required in their problem of zero gravity. A finite element method was used by Hu & Joseph (1989) in their extension of the work of Preziosi *et al.* The finite element method seemed to be more efficient than the collocation method. Attempts have been made to test the accuracy and convergence by doubling the number of terms in the present problem. It was found that for such a large system, the numerical error with a double precision calculation dominates the reduced truncation error.

Figure 1 shows the velocity distribution in the basic state for various values of R for the given parameters $l = 10$, $N = 0.018$, and $Q = 0.0013$. These values of N and Q correspond to a water jet in atmosphere at room temperature. Figure 2 plots the growth rates ω_r against the wavenumber of the disturbance for various values of We

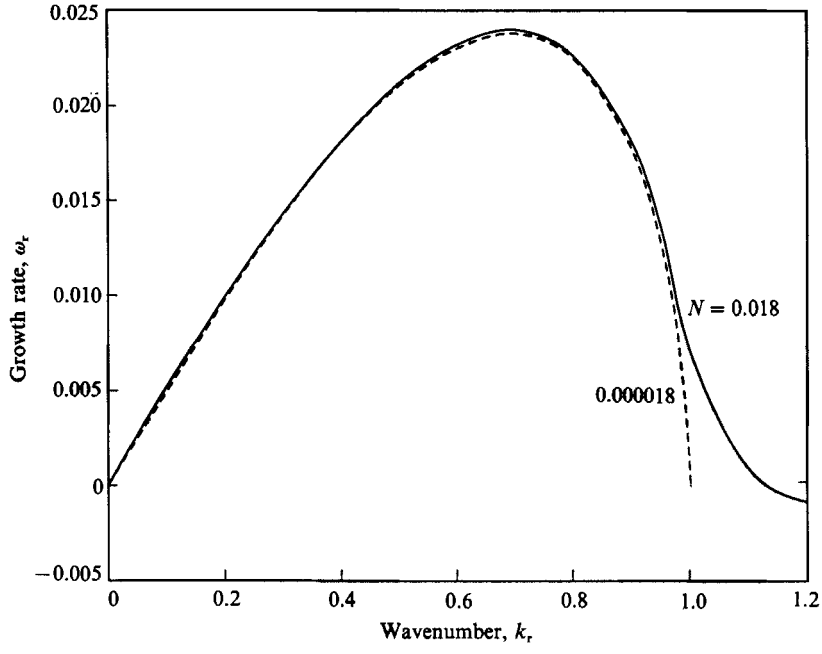

FIGURE 3. Effects of N on the Rayleigh mode. $Q = 0.0013$, $l = 10$, $R = 0$, $Re = 400$, $We = 0.0025$.

for the set of parameters specified in the figure caption. $R = Re/Fr = 0$ signifies the absence of gravity. It is clearly seen that as We is decreased from 0.01 to 10^{-5} in steps, the amplification rates decrease for $k < 1$. For $k > 1$ the trend is reversed, although the growth rates are relatively small. The reversal of the trend can be easily understood by looking at the last term in (4*e*). The factor $(1-k^2)\xi$ in this term arises from the curvature of the interface. The ξ-term is associated with the interfacial curvature along a direction perpendicular to the jet axis which gives rise to the necking at $\xi < 0$ and expansion at $\xi > 0$. The $-k^2\xi$ term is of opposite sign and is associated with the curvature in the axial direction. This curvature tends to pull the displaced interface back to its basic state position. When $k < 1$, the former destabilizing pinching effect dominates the latter stabilizing effect. When $k > 1$ the role of surface tension is reversed. For the given parameters the jet instability is clearly due to the Rayleigh mode of capillary pinching, since the maximum growth rate occurs at $k < 1$. As We is decreased further from 0.0001, the wavelengths corresponding to the maximum growth rates gradually shift to the region $k > 1$. This is exemplified by the curve for $We = 10^{-5}$ in figure 2. Then the instability judged by the maximum amplification rate is no longer due to capillary pinching, but due to the Taylor mode. This mode will be expounded more clearly later when gravity is taken into account. Contrary to the dramatic effect of surface tension on the Rayleigh mode, the air viscosity has little effect on this mode, as can be seen in figure 3, except when $k > 1$ where a relatively large gas viscosity tends to destabilize the jet. Figure 4 shows that an increase in gas density of a hundred-fold can assist the capillary pinching only slightly. The range of Q in this figure corresponds to the water jet in air of pressure ranging from 1 to 100 atmospheres. Figure 5 shows the effect of Re on the Rayleigh mode. As the viscous force is increased relative to the inertia force in the jet, both the wavenumber and the growth rate corresponding to the most

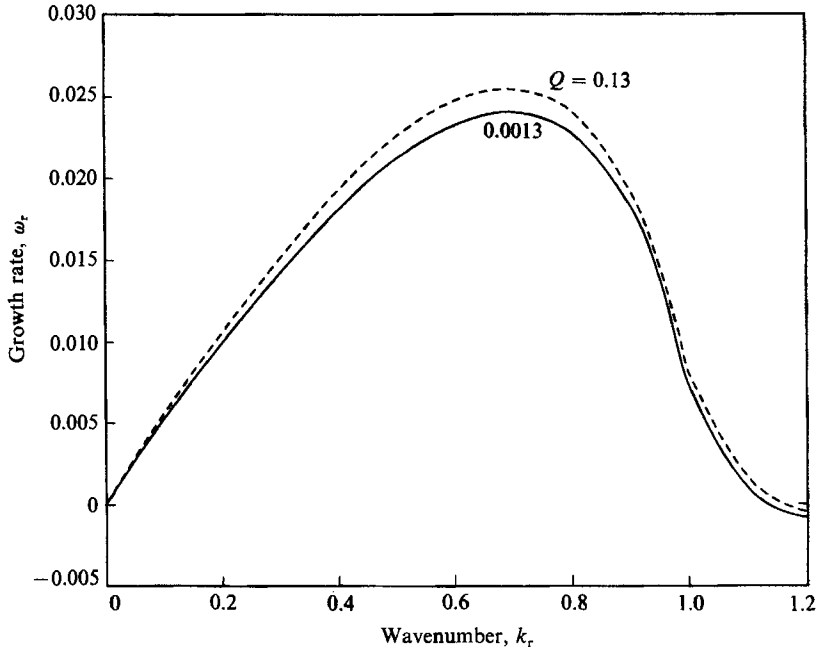

FIGURE 4. Effects of Q on the Rayleigh mode. $l = 10$, $N = 0.018$, $R = 0$, $We = 0.0025$, $Re = 400$.

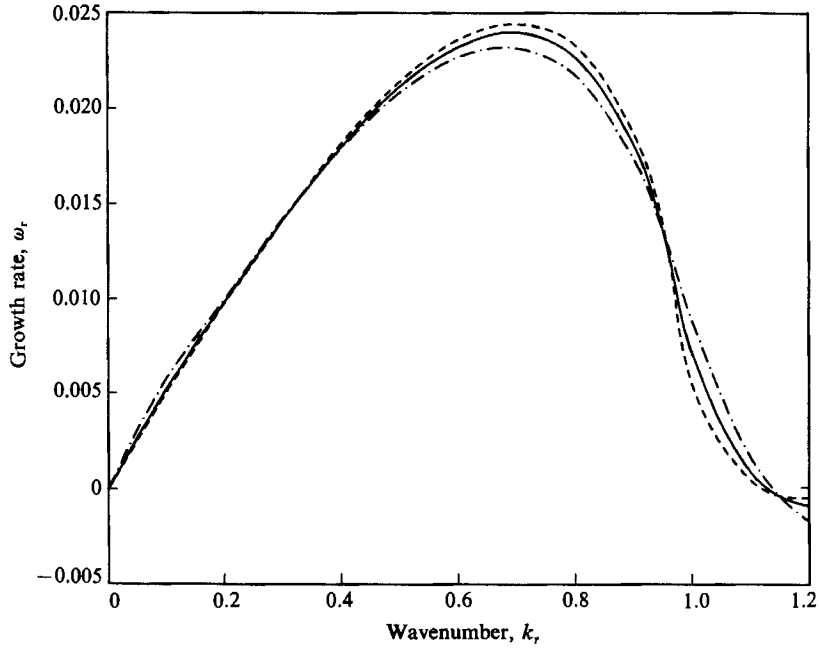

FIGURE 5. Effects of Re on the Rayleigh mode. $l = 10$, $N = 0.018$, $Q = 0.0013$, $R = 0$, $We = 0.0025$. —·—, $Re = 200$; ——, $Re = 400$; – – –, $Re = 800$.

amplified wave decrease. The same trend was found by Chandrasekhar. Figure 6 shows the effect of l. As l is decreased, the shear rates in the basic state increase. This increase results in a slight increase in the amplification rate for $k < 1$ where the capillary pinching remains the dominant mechanism of instability. The destabilizing

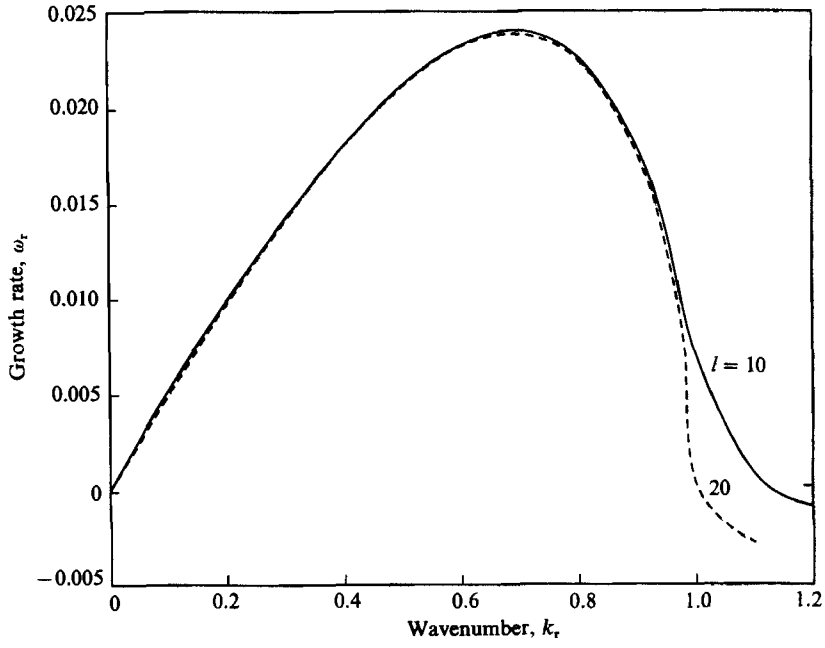

FIGURE 6. Effects on the Rayleigh mode. $N = 0.018$, $Q = 0.0013$, $R = 0$, $We = 0.0025$, $Re = 400$.

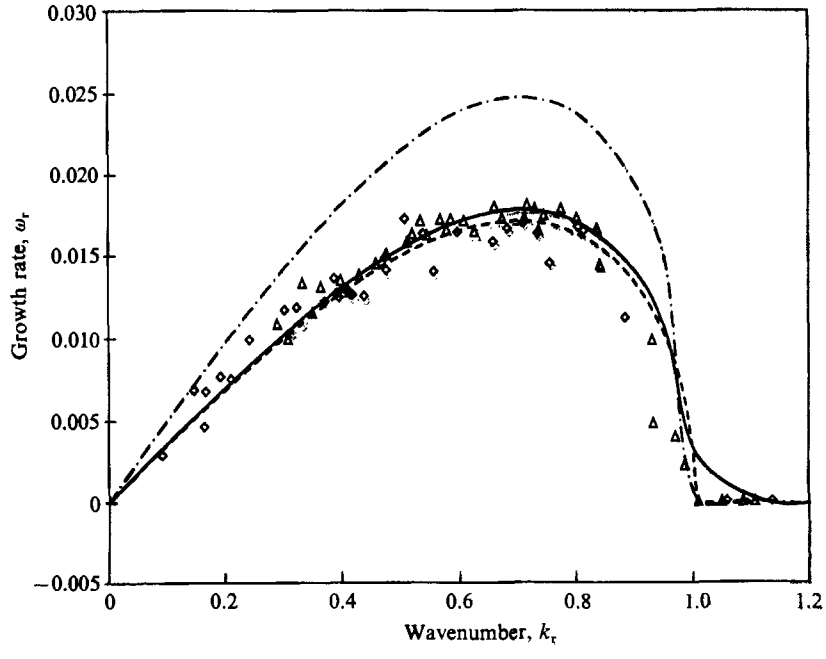

FIGURE 7. Comparisons of theories with experiments. ——, present work, $We = 0.0013$; — — —, present work, $We = 0.0025$; ---, Rayleigh; △, Goedde & Yuen; ◇, Donnelly & Glaberson. For the present work, $Re = 3000$, $Re/Fr = 0$, $Q = 0.0013$, $N = 0.018$, $l = 10$.

effect of the basic state shear rate is significant for shorter waves for which $k > 1$. Comparisons between our theoretical results and the experimental results of Goedde & Yuen (1970) and that of Donnelly & Glaberson (1966) are made in figure 7. Unfortunately, the values of We and Re corresponding to the experimental points

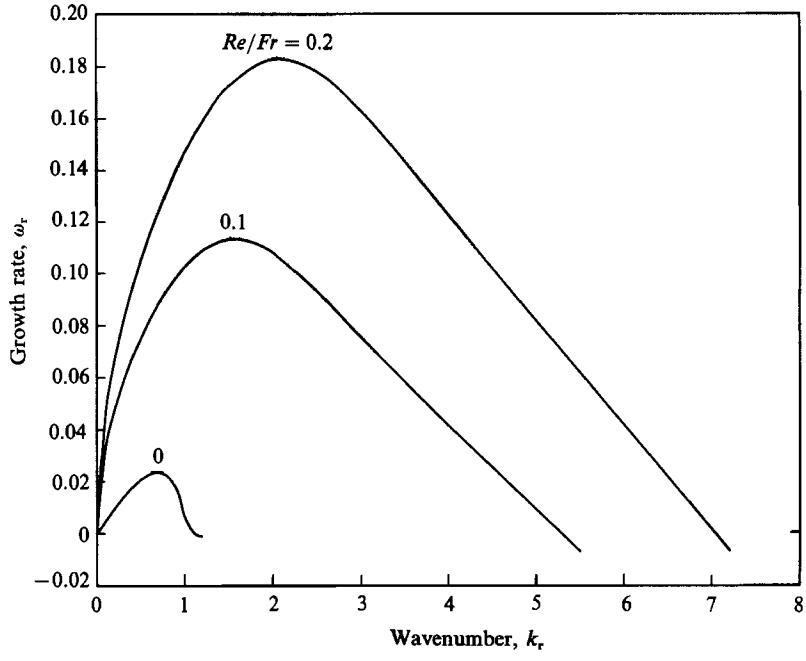

FIGURE 8. Emergence of the Taylor mode. $l = 10$, $N = 0.018$, $Q = 0.0013$, $We = 0.0025$, $Re = 400$.

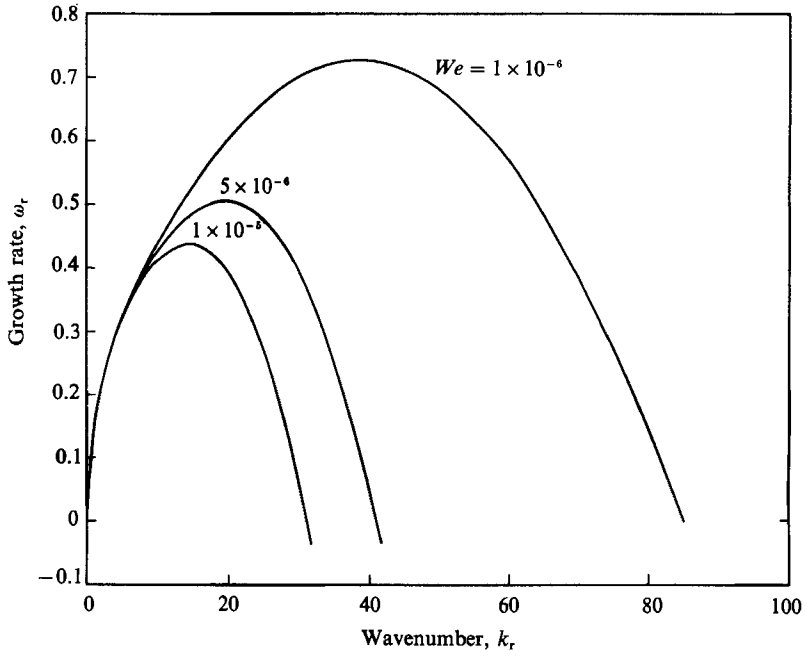

FIGURE 9. Effects of We on the Taylor mode. $l = 10$, $N = 0.018$, $Q = 0.0013$, $R = 0.2$, $Re = 400$.

were not reported. Two amplification curves were obtained from our theory with the parameters corresponding to the lower range of the jet velocity reported by Goedde & Yuen. Rayleigh's amplification curve is also included in this figure for comparison. While the slope of Rayleigh's curve has a discontinuity at $k = 1$, the jet is neutrally

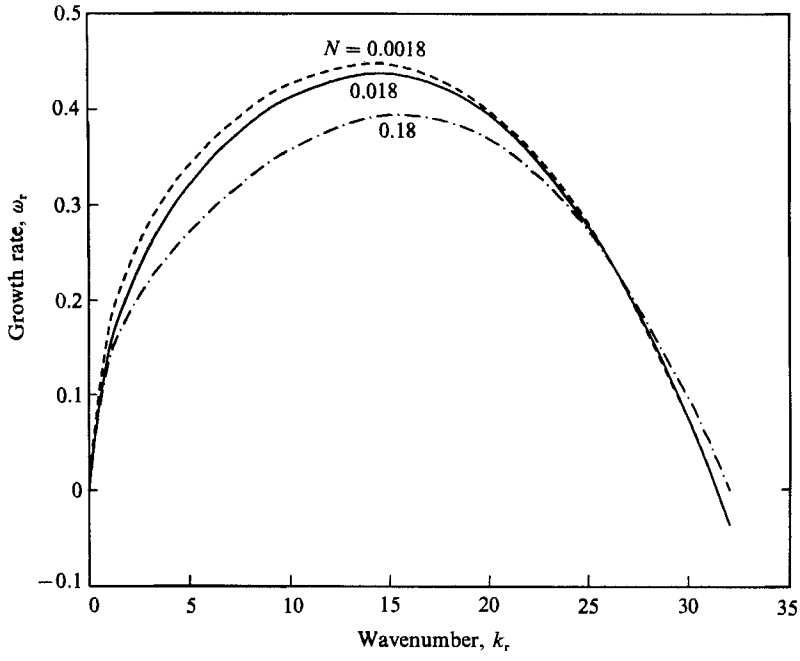

FIGURE 10. Effects of N on the Taylor mode. $l = 10$, $Q = 0.0013$, $We = 10^{-5}$, $R = 0.2$, $Re = 400$.

stable for $k > 1$, our curve is continuous in slope and gives negative ω_r for $k > 1.1$. The good agreement between the experiments and our curve for $Re = 3000$ and $We = 0.0013$ and Rayleigh's curve, which is independent of We at $Re = \infty$ is probably fortuitous. It has already been shown that the amplification curves depend very sensitively on We, although less so on other parameters. For a better comparison with theories, complete records of all relevant parameters (l, Q, We, Re, N) for each observation of (ω_r, ω_i, k) are needed. Figure 8 demonstrates the effect of R. The wavenumber corresponding to the maximum amplification rate is shifted from the region $k < 1$ to the region $k > 1$ as R as increased from 0. Moreover, the amplification rates for the non-vanishing values of R are orders of magnitude larger than that for the Rayleigh jet for which $R = 0$. Hence the majority of unstable disturbances for $R \neq 0$ belong to $k > 1$, and their instability mechanism, as was explained in connection with figure 2, is no longer the capillary pinching. Here, we see the emergence of the Taylor mode associated with the interfacial stress fluctuation. Figure 9 further demonstrates the stabilizing effect of the interfacial tension. As We is decreased to values much smaller than Q, both the amplification rates and the wavenumber of the unstable spectrum are increased dramatically. It is seen that the most unstable disturbances of Taylor's atomization mode are of wavelength several orders of magnitude smaller than the jet radius. Moreover, the wavelengths near the maximum growth rates of the amplification curves all scale with the capillary length $a = 2\pi S/\rho_2 W_0^2 R_1$. This can be verified by showing that the following equation is satisfied with the values of the wavenumber k_m, corresponding to the maximum growth rate, taken from each curve of figure 10,

$$(2\pi R_1/k) \approx a \equiv 2\pi S/\rho_2 W_0^2 R_1 = 2\pi R_1 (We/Q).$$

Recall that in the Rayleigh mode, the most amplified waves scale with R_1 in length. Contrary to the situation in the Rayleigh mode (cf. figure 3), the air viscosity has a

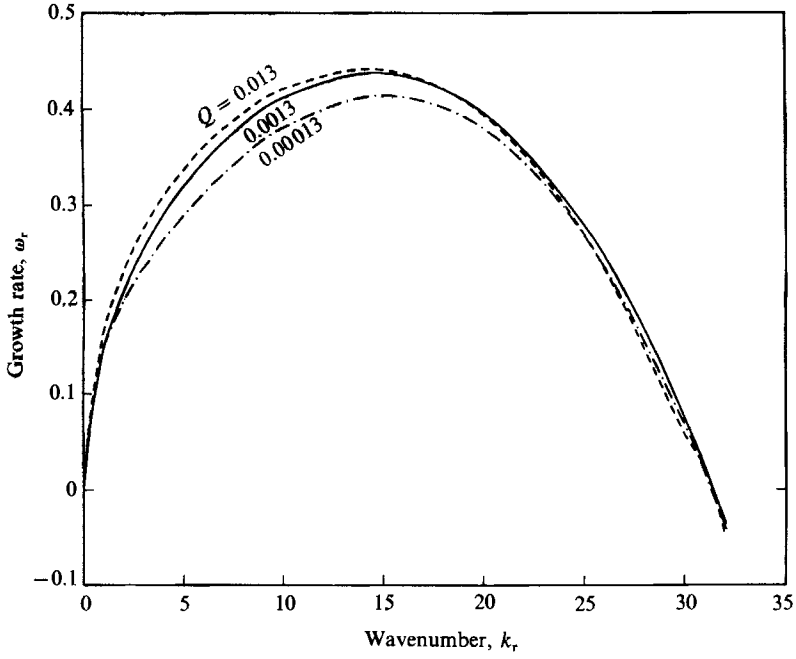

FIGURE 11. Effects of Q on the Taylor mode. $l = 10$, $N = 0.018$, $We = 10^{-5}$, $R = 0.2$, $Re = 400$.

more significant effect on the atomization mode, as can be seen in figure 10. When N is increased from 0.0018 to 0.018 the disturbances for which $k < 23$ are damped while the disturbances for which $k > 23$ are amplified. This seems to reflect the fact that the enhancement of the amplification rate owing to the relative increase in gas viscosity more than compensates for the decrease in the damping rate owing to the relative decrease in the liquid viscosity for shorter waves such that $k > 23$. The reverse is true for longer waves for which $k < 23$. This also reveals the crucial roles played by the gas shear stress in the generation of small droplets. Neglecting the gas viscosity, Lin & Kang (1987), and Lin & Creighton (1990) showed that only pressure fluctuation can generate short waves scaling with capillary length. It is clear now that the interfacial shear and pressure fluctuations are equally capable of generating short waves scaling with the capillary length. This view is further substantiated by figures 11 and 12 which show qualitatively the same behaviour as figure 10, when the ratio of inertia force relative to viscous force is raised respectively by raising the value of Q and Re. Figure 13 shows the destabilizing effect of the basic state shear rate on the Taylor mode. A large basic state shear rate at the interface requires a large shear stress fluctuation when the interface fluctuates from the unperturbed cylindrical surface, in order to satisfy the condition of vanishing shear force at the interface (cf. Hinch 1984; Kelly *et al.* 1989). This large shear-stress fluctuation inevitably brings about a large pressure fluctuation, and causes the growth rate to increase. In contrast to the situation in figure 6, the radius ratio l has a very significant effect on the Taylor mode (figure 14). A decrease in l brings about a larger basic state shear rate which again results in an increase in the growth rate. Unlike the case of $Q = 1$, $We = 0$, and $N < 1$ investigated by Joseph *et al.*, we did not find stability near $k = 0$ when $l \to 1$ for finite values of We and $Q \ll 1$. However, when we put $We = 0$, $Q = 1$, $N = 0.5$, $R = 0$ and $Re = 27.2$ we did find that the jet is stable for

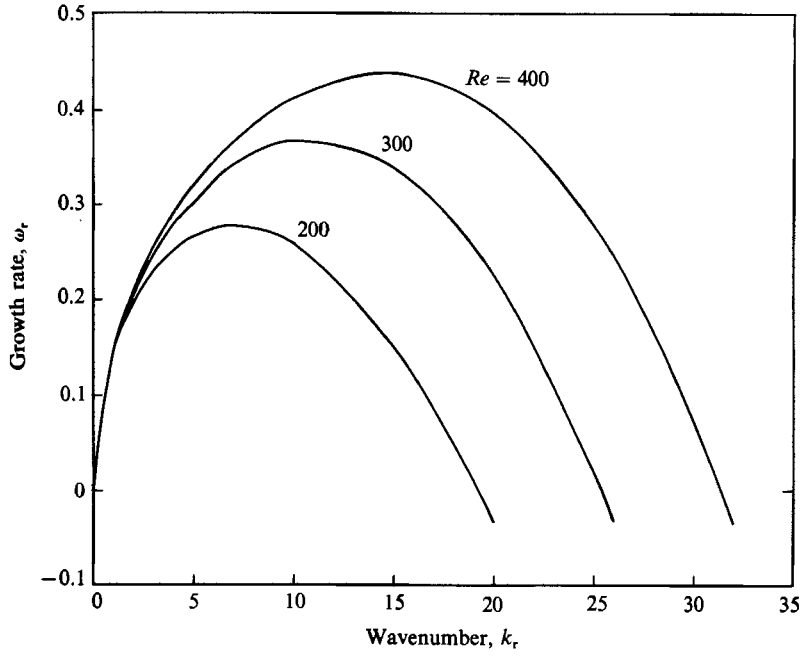

FIGURE 12. Effects of Re on the Taylor mode. $l = 10$, $N = 0.018$, $Q = 0.0013$, $We = 10^{-5}$, $Fr = 2000$.

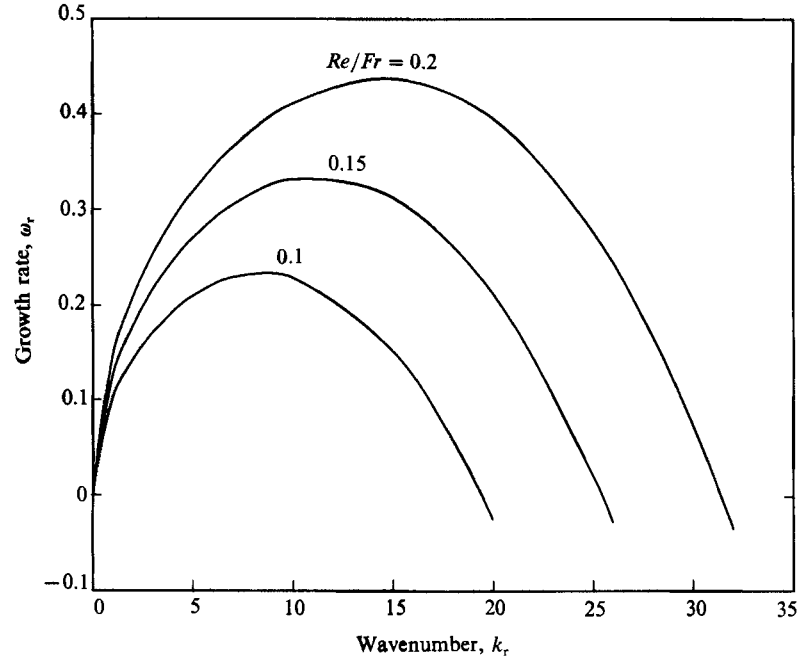

FIGURE 13. Effects of R on the Taylor mode. $l = 10$, $N = 0.018$, $Q = 0.0013$, $We = 10^{-5}$, $Re = 400$.

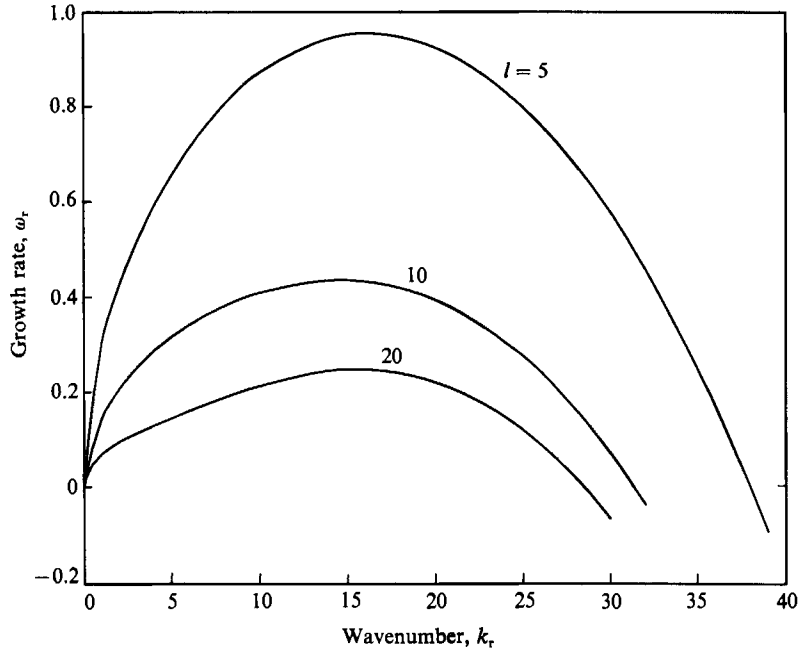

FIGURE 14. Effects of l on the Taylor mode. $N = 0.018$, $Q = 0.0013$, $We = 10^{-6}$, $R = 0.2$, $Re = 400$.

$6 < k$ and $k < 0.7$. This is consistent with the results of Joseph *et al.* (1984). Hooper & Boyd (1987) and Renardy (1985) also found a similar stable region for planar Couette flow of two superposed fluids of different viscosities but of the same density.

5. Discussion

It should be pointed out that the instability waves near $k = 0$ in the present work are not of the type of Yih (1967), since Yih's long shear waves are not apparent when $N < 1$ (cf. Hooper & Boyd 1987). The stability analysis of a viscous liquid jet in an ambient gas reveals that there are two distinct mechanisms of the jet break-up. The first is that of the Rayleigh mode by capillary pinching, and the second is that of the Taylor mode by interfacial shear and pressure fluctuations. The theory is not yet fully substantiated by experiments. The present theory predicts that the growth rate of disturbances in the Rayleigh mode increases significantly with the Weber number as it should, since the instability is due to capillary pinching. Unfortunately, the known experiments in the Rayleigh mode regime failed to record the values of relevant parameters including We for each experimental point. Only the ranges of velocity, temperature, and jet diameter were reported. Thus only the ranges of the parameters encountered in experiments can be estimated. This deprives us of a more complete comparison. Consequently the apparent agreement between experiments and the present theory with $We = 0.0013$ and $Re = 3000$, and with the Rayleigh theory remain fortuitous. This value of We and the values of the rest of parameters used in figure 7 are in the lower end of the parameter range estimated from the reported experimental data. It is possible that most of the experimental points were obtained in the lower range of the parameters encountered in experiments. The theoretical results on the Taylor mode are only qualitatively substantiated by the

experiments of Reitz & Bracco (1982). The average diameters of their atomized droplets all seem to scale with the capillary length, as predicted by our theory. Careful measurements of (ω_r, ω_i, k) for various given sets (We, Re, Q, N, l) are required for a better comparison with the theory for both modes. There may exist other modes of instability in the parameter ranges not considered in this work. A possible third mode which may correspond to a dripping jet (cf. Lin & Lian 1989) is yet to be explored by considering the convective and absolute instabilities of spatially growing disturbances when $We \gg Q$. The known analysis of absolute and convective instabilities of a jet all ignore the effect of gas viscosity (Leib & Goldstein 1986*a*, *b*; Lin & Lian 1989). Blennerhassett (1980) showed that Tollmien–Schlichting waves are more stable than the interfacial waves in two superposed viscous fluids flowing over a plane. The same situation appears to happen here. The Tollmien–Schlichting wave will probably not appear until Re is raised to a value much greater than those considered in this work.

While the present analysis also applies to the case of $N > 1$, the computation for this case has not yet been carried out. The extension of the present analysis to the case of non-axisymmetric disturbances is quite straightforward. The nonlinear stability analysis of the linearly unstable disturbances described in this work will be useful for many industrial processes which utilize the mechanisms of the jet breakup either in Taylor's atomization mode or Rayleigh's ink-jet mode.

This work was supported in part by grant no. DAAL03-89-K-0179 of ARO, grant no. MSM-8817372 of NSF and a New York State Science Foundation Grant. The computation was carried out with the computer facility at Clarkson University and with the Cornell National Computer facility, which is funded by the NSF, the States of New York, and IBM Corporation.

REFERENCES

BLENNERHASSETT, P. J. 1980 *Phil. Trans. R. Soc. Lond.* A **298**, 451.

CHANDRASEKHAR, S. 1961 *Hydrodynamic and Hydromagnetic Stability*, p. 537. Oxford University Press.

CHEN, K., BAI, R. & JOSEPH, D. D. 1990 *J. Fluid Mech.* **214**, 251.

DONNELLY, R. J. & GLABERSON, W. 1966 *Proc. R. Soc.* A **290**, 547.

DRAZIN, P. G. & REID, W. H. 1981 *Hydrodynamic Stability*. Cambridge University Press.

GOEDDE, E. F. & YUEN, M. C. 1970 *J. Fluid Mech.* **40**, 495.

HINCH, E. J. 1984 *J. Fluid Mech.* **128**, 507.

HOOPER, A. P. & BOYD, W. G. C. 1987 *J. Fluid Mech.* **179**, 201.

HU, H. H. & JOSEPH, D. D. 1989 *J. Fluid Mech.* **205**, 359.

JOSEPH, D. D., RENARDY, M. & RENARDY, Y. 1984 *J. Fluid Mech.* **141**, 309.

KELLER, J. B., RUBINOW, S. I. & TU, Y. O. 1972 *Phys. Fluids* **16**, 2052.

KELLY, R. E., GOUSSIS, D. A., LIN, S. P. & HSU, F. K. 1989 *Phys. Fluids* A **12**, 819.

KAUFMAN, L. C. 1974 *SIAM J. Num. Anal.* **11**, 997.

MULLER, D. C. 1956 *Math. Tables Aids Comput.* **10**, 208.

LEIB, S. J. & GOLDSTEIN, M. E. 1986*a* *J. Fluid Mech.* **168**, 479.

LEIB, S. J. & GOLDSTEIN, M. E. 1986*b* *Phys. Fluids* **29**, 952.

LIN, S. P. & CREIGHTON, B. 1990 *J. Aero. Sci. Tech.* **12** (3), (to appear).

LIN, S. P. & KANG, D. J. 1987 *Phys. Fluids* **30**, 2000.

LIN, S. P. & LIAN, Z. W. 1989 *Phys. Fluids* A **1**, 490.

LIN, S. P. & LIAN, Z. W. 1990 *AIAA J.* **28**, 120.

PREZIOSI, L., CHEN, K. & JOSEPH, D. D. 1989 *J. Fluid Mech.* **201**, 323.

RAYLEIGH, LORD 1879 *Lond. Math. Soc.* **10**, 361.

REITZ, R. D. & BRACCO, F. V. 1982 *Phys. Fluids* **25**, 1730.

RENARDY, Y. 1985 *Phys. Fluids* **28**, 3441.

SMITH, M. K. 1989 *Phys. Fluids* A **1**, 494.

TAYLOR, G. I. 1963 *The Scientific Papers of Sir Geoffrey Ingram Taylor*, vol. 3, No. 25. Cambridge University Press.

TOMOTIKA, S. 1934 *Proc. R. Soc. Lond.* A **146**, 501.

YIH, C. S. 1967 *J. Fluid Mech.* **27**, 337.